

Signature of two-dimensional conduction on crystal surface of Mott insulator NiS_2

Xue-Bin Dong(董学斌), Meng Lyu(吕孟), Yi-Bo Wang(王一博), Yang Liu(刘洋), Jin-Ying Yang(杨金颖), Xing-Chen Liu(刘星辰), Bin-Bin Wang(王彬彬), Xi-Yang Li(李西阳), En-Ke Liu(刘恩克)

Citation: Chin. Phys. B. 35, 097102 (2026). DOI: 10.1088/1674-1056/ae6f98 |
CSTR: 32038.14.CPB.ae6f98
http://cpb.iphy.ac.cn; http://iopscience.iop.org/cpb

What follows is a list of articles you may be interested in

Quantum phase transition of two-dimensional NdOCl

Chenfeng Liu(刘晨峰), Wangyang Du(杜汪洋), Fei Gao(高飞), Hongshuai Tao(陶红帅)
Chin. Phys. B. 35, 087103 (2026). DOI: 10.1088/1674-1056/ae1566 | CSTR: 32038.14.CPB.ae1566

Single crystal growth and electronic structure of Fe-doped $Sr_3Ir_2O_7$

Muhammad Waqas, Bingqian Wang(王冰倩), Shuting Peng(彭舒婷), Jianchang Shen(沈建昌), Linwei Huai(淮琳崴), Xiupeng Sun(孙秀鹏), Yu Miao(缪宇), Pelda Uzun, Runqing Luan(栾润青), Zikun Feng(冯梓琨), Dai Pan(潘岱), Xinru Yong(勇欣茹), Hongxu Sun(孙鸿绪), Zhipeng Ou(欧志鹏), Junfeng He(何俊峰)
Chin. Phys. B. 34, 107101 (2025). DOI: 10.1088/1674-1056/adda0b | CSTR: 32038.14.CPB.adda0b

Strain tuning of charge density wave and Mott-insulating states in monolayer VTe_2

Wenqian Tu(涂文倩), Run Lv(吕润), Dingfu Shao(邵定夫), Yuping Sun(孙玉平), Wenjian Lu(鲁文建)
Chin. Phys. B. 34, 097103 (2025). DOI: 10.1088/1674-1056/ade8e0 | CSTR: 32038.14.CPB.ade8e0

Quantitative determination of the critical points of Mott metal–insulator transition in strongly correlated systems

Yuekun Niu(牛月坤), Yu Ni(倪煜), Jianli Wang(王建利), Leiming Chen(陈雷鸣), Ye Xing(邢晔), Yun Song(宋筠), Shiping Feng(冯世平)
Chin. Phys. B. 33, 017102 (2024). DOI: 10.1088/1674-1056/ad0719

Mottness, phase string, and high-T_c superconductivity

Jing-Yu Zhao(翁征宇), Zheng-Yu Weng(翁征宇)
Chin. Phys. B. 31, 087104 (2022). DOI: 10.1088/1674-1056/ac7a14

RAPID COMMUNICATION

Signature of two-dimensional conduction on crystal surface of Mott insulator NiS_2

Xue-Bin Dong(董学斌)[1,2], Meng Lyu(吕孟)[1], Yi-Bo Wang(王一博)[1,2], Yang Liu(刘洋)[1,2], Jin-Ying Yang(杨金颖)[1], Xing-Chen Liu(刘星辰)[1,2], Bin-Bin Wang(王彬彬)[1], Xi-Yang Li(李西阳)[1], and En-Ke Liu(刘恩克)[1,†]

[1] *Beijing National Laboratory for Condensed Matter Physics, Institute of Physics, Chinese Academy of Sciences, Beijing* 100190, *China*
[2] *School of Physical Sciences, University of Chinese Academy of Sciences, Beijing* 100049, *China*

(Received 31 March 2026; revised manuscript received 13 May 2026; accepted manuscript online 19 May 2026)

Exploring low-dimensional electronic states is a frontier in condensed matter physics, particularly in systems with insulating bulks and conducting surfaces. NiS_2 is a prototypical Mott insulator where macroscopic surface conduction has long been observed, yet its microscopic transport dimensionality (1D vs. 2D) remains an ongoing debate. This work addresses this puzzle by providing transport signatures that support an intrinsic 2D origin for this behavior. Below $T^* \sim 100$ K, the resistivity develops a plateau conforming to a 2D Mott-type variable-range hopping. Simultaneously, the angle-dependent magnetoresistance reveals symmetries consistent with the (001) surface lattice, suggesting 2D transport rather than oriented 1D channels. This 2D character is further supported by the resilience of surface conduction under slight doping-induced disorder, in contrast to inherently unstable 1D systems. These findings help understand the physical origin of the surface transport mechanism in Mott insulator NiS_2.

Keywords: Mott insulator, surface conduction, variable-range hopping, magnetotransport

PACS: 71.30.+h, 73.50.–h, 72.20.Ee, 75.47.–m

DOI: 10.1088/1674-1056/ae6f98 **CSTR:** 32038.14.CPB.ae6f98

Over the past decades, pyrite-type transition metal dichalcogenides MS_2 (M = Fe, Co, etc.) have garnered sustained research attention.[1–4] These MS_2 compounds exhibit exotic electronic states with intriguing physical phenomena, such as the magnetic Weyl semimetal CoS_2 with large linear positive magnetoresistance and the superconductor CuS_2 that hosts a charge density wave.[5–10] While this family of materials shares similar non-interacting electronic structures, their diverse properties are driven primarily by differences in charge filling, highlighting the decisive role of crystal-field effects and electron correlation. Among them, NiS_2 serves as a prototypical Mott–Hubbard insulator.[11,12] In such a system, strong on-site Coulomb repulsion drives a metal-to-insulator transition, a phenomenon that, along with complex antiferromagnetic orders, has been central to previous studies on its bulk correlation physics.[13–20] However, a long-standing transport anomaly persists in NiS_2, characterized by a plateau-like feature in the temperature-dependent resistivity $\rho(T)$ that emerges despite the presence of the bulk charge-transfer gap.[16,21–23] Such a conflict has prompted efforts to uncover the underlying physical mechanism.

While early works attributed this anomaly to defect-induced impurity bands,[24] subsequent investigations into transport properties have established a phenomenological surface conduction (SC) mechanism.[23,25–30] Theoretically, NiS_2 has been predicted to host an obstructed atomic insulator phase, where the shift of Wannier charge centers from atomic sites leads to intrinsic 2D conduction on specific as-cleaved surfaces.[31–34] This framework provides a rigorous explanation for the observed SC beyond simple surface degradation. Nevertheless, a recent scanning tunneling spectroscopy study revealed the existence of atomic-scale 1D-like conduction channels rather than a uniform 2D metallic surface layer, challenging the prevailing picture.[35] This discrepancy raises a fundamental question: does the macroscopic SC arise from an intrinsically 2D electronic state or the 1D conducting channels? Discriminating between these two scenarios is essential for revealing the physical origin of SC in NiS_2.

In this paper, we investigate the microscopic dimensionality of SC in NiS_2 through a series of transport signatures, which indicate a 2D nature for this emergent behavior. Below $T^* \sim 100$ K, the $\rho(T)$ quantitatively follows a 2D Mott variable-range hopping (VRH) mechanism. Angle-dependent magnetoresistance (ADMR) further reveals a two-fold symmetry consistent with the surface crystalline plane across multiple rotation geometries, providing macroscopic evidence for a pervasive 2D conduction sheet rather than oriented 1D channels. Furthermore, the persistence of surface conduction against Cu/Co substitution-induced disorder ($\sim 0.6\%$) contrasts with the strong localization tendency inherently ex-

†Corresponding author. E-mail: ekliu@iphy.ac.cn

© 2026 Chinese Physical Society and IOP Publishing Ltd. All rights, including for text and data mining, AI training, and similar technologies, are reserved.

pected for 1D electronic systems. These findings also illustrate the utility of transport analysis in probing the dimensionality of electronic states in insulating materials.

NiS_2 single crystals and Cu/Co-doped variants were synthesized using the Te-flux method. Elemental reagents of nickel (99.99%), sulfur (99.99%), and tellurium (99.99%) were combined at a 1:2:14 molar ratio in a quartz tube and sealed under vacuum. The ampoules were slowly heated to 1073 K, held for 6 h, and then cooled to 773 K at a rate of 1.25 K/h (over 10 days). Excess flux was removed by centrifugation at 773 K. The crystal structure and orientation were characterized by x-ray diffraction (XRD) using Cu K_α radiation. Elemental stoichiometry was examined by energy-dispersive x-ray spectroscopy (EDS, Hitachi S-4800). To resolve the intrinsic surface transport, measurements were conducted on three sample configurations: as-grown, as-polished, and mechanically as-cleaved. Polishing was employed to define precise slab geometries for resistivity calculations, while cleavage was used to expose pristine (001) surfaces to minimize extrinsic degradation. All samples were taken from the same batch. Electrical transport measurements were performed using a standard four-probe method in a physical property measurement system (PPMS, Quantum Design).

The investigation began with validating the structural and stoichiometric integrity of NiS_2 single crystals to ensure reliability. This compound crystallizes in a cubic structure (space group $Pa\bar{3}$, No. 205), featuring Ni atoms occupying the face-centered cubic sublattices and S-dimers oriented along body-diagonal directions (Fig. 1(a)). Magnetization measurements and neutron diffraction reveal an antiferromagnetic order in NiS_2, with a Néel temperature $T_N = 39$ K and a magnetic moment of 1 μ_B/Ni, followed by the development of weak ferromagnetism with a Curie temperature $T_C = 30$ K.[36,37] Figure 1(b) displays the EDS of our samples, which reveals a near-stoichiometric atomic ratio of Ni : S = 1 : 1.99 and demonstrates elemental homogeneity. Although slight stoichiometric deviation indicates a degree of disorder, the characteristic insulating property remains well-preserved (see Fig. 2). This robustness stems from the dominance of Mott physics in the bulk state, as opposed to a non-interacting band insulator arising from charge filling in bands.[12] Figure 1(c) shows the XRD pattern of the as-grown NiS_2 single crystals. Only (00l) Bragg peaks are observed, indicating the (001) orientation of the exposed surface (Fig. 1(c)). To verify the hallmark transport anomaly, $\rho(T)$ was characterized using a slab fabricated from a (001)-oriented single crystal (Fig. 1(d)). The curve initially exhibits a negative temperature coefficient of resistivity (TCR) below 300 K, followed by a sign reversal of the TCR around T^* that resembles an insulator-to-metal transition. T^* marks the crossover from high-temperature thermal activation to a low-temperature transport anomaly regime in log-log plots. This negative TCR reflects the gapped bulk state, while the low-temperature resistivity manifests as a plateau (inset of Fig. 1(d)), representing a transport anomaly previously attributed to SC.[23,27,28] Here, the plateau denotes (weakly) T-dependent low-temperature resistivity in log–log plots, in contrast to bulk thermal activation behavior. In the following, we move beyond the phenomenological identification of surface transport to investigate its dimensionality through scaling analysis in $\rho(T)$, ADMR symmetry, and disordered transport.

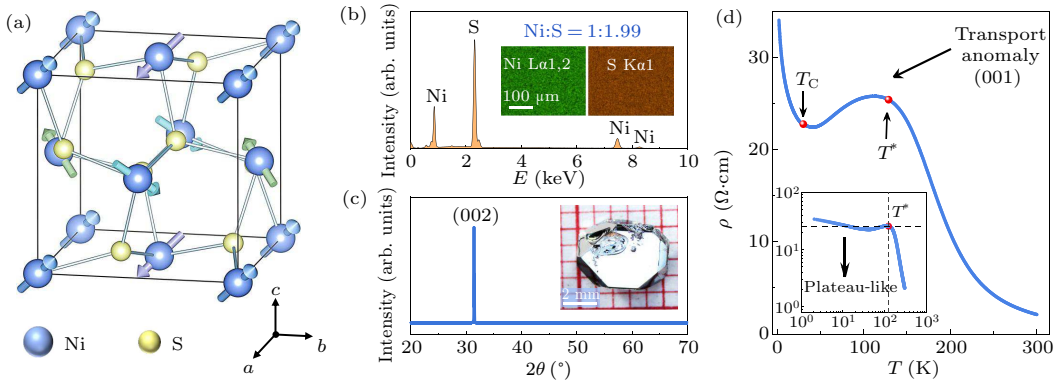


Fig. 1. Crystal structure and basic characterization of NiS_2. (a) Crystal structure and magnetic structure of NiS_2. (b) EDS of a NiS_2 single crystal. Insets: Corresponding elemental mapping for Ni and S. (c) XRD pattern of the exposed surface of the NiS_2 single crystal. Inset: Optical image of a typical single crystal. (d) The $\rho(T)$ of a as-polished NiS_2 single crystal (sample S01) sample oriented along the (001) plane, with I flowing along [100].

To elucidate the surface transport, we performed a comparative analysis on $\rho(T)$ data measured from single crystals with various surface treatments. The data are presented as normalized resistance $R/R_{300\,K}$ to effectively eliminate sample-specific geometric uncertainties (Fig. 2(a)). In the high-temperature regime ($T > T^*$), all curves overlap onto a single trace, illustrating the intrinsic insulating bulk. As shown in the Arrhenius plot (inset of Fig. 2(a)), the curve follows the thermal activation law: $R = R_0 \cdot \exp(\Delta/k_B T)$, where k_B is the Boltzmann constant, R_0 is a fitting factor, and Δ denotes activation energy. The extracted Δ of all samples ranges from 90.5 meV to 97.5 meV, in agreement with re-

ported values,[22,23,29] also demonstrating its independence of surface processing condition. Nevertheless, a clear discrepancy emerges among the samples at low temperatures, indicating that the transport is dependent on surface condition below T^* (Fig. 2(a)). In particular, the as-polished sample (S01) shows a significantly enhanced SC contribution, as demonstrated by its smaller $R/R(300\ \mathrm{K})$ below T^* compared with the other samples (Fig. 2(a)). Furthermore, T^* differs across samples, with values of 92 K, 106 K, and 130 K for the as-grown, as-cleaved, and as-polished samples, respectively. This distinct variation reflects the competition between surface and bulk transport behaviors. In contrast, T_C remains nearly unchanged, which corresponds to the intrinsic bulk properties of NiS_2. Such an enhancement, previously observed in NiS_2,[23] likely originates from surface microstructural defects like polishing-induced cracks, similar to discussion in other surface-conducting systems such as SmB_6.[38,39]

To further probe the intrinsic nature of the resistivity plateau, we normalized the resistance data to $R/R_{2\ \mathrm{K}}$ (Fig. 2(b)). The curves for the as-grown and as-cleaved samples show excellent overlap at low temperatures, suggesting that they share a common transport mechanism. Based on this equivalence, the as-grown sample (S02) is selected as a representative for the subsequent detailed analysis. Given that a distinct negative TCR persists below T^* for as-grown S02 (see Fig. S1(b) in supplementary information), we applied the Arrhenius equation to check for a potential thermal activation gap in this regime. As shown in Fig. 2(c), the Arrhenius plot exhibits good linearity only in the regime below 5 K. Moreover, the extracted gap $\Delta \approx 1.2$ K is comparable to the thermal energy $k_B T$ in this temperature range, reflecting that the transport behavior in the plateau regime cannot be explained by a well-defined activation gap.

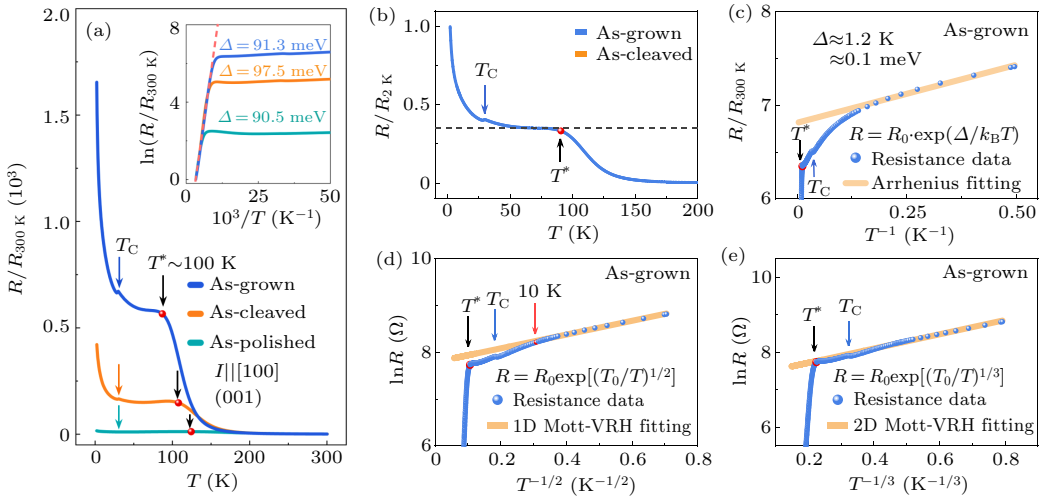


Fig. 2. Evolution of the dominant conduction mechanism from thermal activation to Mott-type VRH in NiS_2. (a) $R/R_{300\ \mathrm{K}}$ for as-polished (S01), as-grown (S02), and as-cleaved (S03) samples. Inset: Arrhenius plot with a linear fitting to extract Δ. (b) Temperature dependence of $R/R_{2\ \mathrm{K}}$ for S02 and S03. (c)–(e) Fitting of the resistance data below T^* for S02 using the Arrhenius equation (c), the Mott-type VRH equation with $d = 1$ (d) and $d = 2$ (e), respectively.

Having ruled out conventional thermal activation via Arrhenius analysis, we further adopt the Mott VRH mechanism to analyze the low-temperature transport. Considering inherent sulfur deficiency and related disorders in real NiS_2 crystals, diffusive carrier transport is expected to be influenced by Anderson localization.[40,41] In disordered systems, Mott-type VRH commonly occurs, wherein charge carriers tunnel between localized states with energy-dependent hopping ranges maximizing tunneling probability.[42,43] Within the Mott-VRH framework, the $\rho(T)$ follows a dimensionality-dependent power-law relation: $\rho = \rho_0 \cdot \exp(T_0/T)^{1/(d+1)}$, where ρ_0 is the pre-exponential factor, T_0 is the characteristic temperature and d denotes the effective dimensionality of the system.[43] It is worth noting that the VRH model is inapplicable to T-regime with metallic behavior. Therefore, the fitting for the as-grown sample S02 is performed only below T^*, where the TCR remains consistently negative (see Fig. S1(b) in supplementary information). Since R and ρ differ only by a constant geometric factor, the VRH law remains valid for R. Motivated by previous reports of 1D-like features,[30] we first examined the $d = 1$ case (Fig. 2(d)). Although the $\rho(T)$ data appear to follow a $T^{-1/2}$ behavior below 10 K, clear deviations occur as the temperature increases. In contrast, the $\rho(T)$ data show much better agreement with a $T^{-1/3}$ ($d = 2$) dependence over a broad temperature range extending up to T^* (Fig. 2(e)). The slight deviation observed between T^* and T_C likely originates from the onset of non-negligible bulk contributions as the temperature increases. Consequently, these observations support that SC in NiS_2 aligns more closely with a 2D Mott-type VRH mechanism rather than 1D hopping or simple thermal activation.

We then extend our investigation to magneto-transport

properties to gain further insight through the magnetoresistance (MR), defined as $\mathrm{MR} = [R(B) - R(0)]/R(0) \times 100\%$. As shown in Fig. 3(a), a weak negative MR is observed above T^*, where insulating bulk conduction dominates. This negative value is consistent with the suppression of spin-disorder scattering under an applied magnetic field, a behavior reported in other Mott insulators such as $SrCuO_2$.[44] Upon cooling, this negative response gradually diminishes and undergoes a sign reversal near T^*, becoming positive at lower temperatures. The emergence of positive MR below T^* can be reasonably understood within the VRH mechanism, where it originates from the B-induced changes in the localization length and the consequent reduction of hopping probability.[45,46] While negative MR can also occur in 2D VRH systems due to quantum interference between different directed hopping paths,[47] the robust positive sign observed here suggests that the suppression of hopping probability is the dominant mechanism in our samples. The crossover behavior is further clearly exhibited in the temperature dependence of MR (Fig. 3(b)), revealing two distinct regimes of opposite sign with the crossover point coinciding with the onset of the resistivity plateau at T^*. This crossover is consistent with the shift from bulk-dominated to surface-dominated transport.

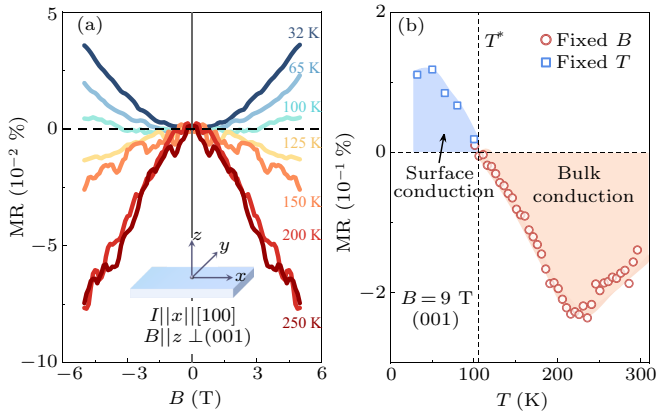


Fig. 3. Temperature-dependent magnetoresistance with sign reversal in NiS_2. (a) MR curves measured over the temperature range of 32–250 K. (b) MR as a function of temperature at 9 T, in the same measurement configuration as in (a). A distinct MR sign crossover is observed near $T^* \sim 100$ K, indicating the transition of conduction mechanism.

To investigate the microscopic dimensionality of SC in NiS_2, we next carried out ADMR measurements on as-cleaved (001) surfaces to resolve its symmetry feature. Distinguishing between 1D and 2D transport via ADMR hinges on the spatial confinement of carrier motion and the anisotropy of the Fermi surface (FS). 1D electronic systems are highly anisotropic, with FSs typically consisting of parallel planes or point pairs that confine transport along specific chain axes. In contrast, 2D systems possess FSs that extend across the surface Brillouin zone (e.g., cylindrical or closed in-plane orbits), yielding symmetries commensurate with the lattice structure. Consequently, ADMR in 1D systems is uniquely sensitive to the orientation of B relative to the conduction axis, because rotating the magnetic field in orthogonal planes yields markedly different angular dependencies. However, for 2D systems with in-plane isotropy such as cubic crystal structures, the transport manifests as invariant responses across orthogonal rotation planes.[48–51] Based on these analyses, two distinct experimental configurations (Figs. 4(a) and 4(d)) were employed on (001)-oriented NiS_2 crystals to systematically discern the dimensionality of the electronic states dominating the low-temperature transport.

The acquired ADMR data reveal a striking consistency between these orthogonal rotation planes. Figure 4 presents ADMR results in polar coordinates, and the corresponding Cartesian coordinate data can be found in Fig. S2 (see supplementary information). In configuration I (Fig. 4(a)), B was rotated within the xz-plane. At 100 K, the ADMR exhibits a $\cos^2\theta$ dependence (Fig. 4(b)). Upon cooling, the profile evolves gradually into an emergent $\sin^2\theta$ dependence that dominates at 35 K (Fig. 4(c)). In configuration II (Fig. 4(d)), B was confined to the yz-plane, remaining transverse to the current at all angles. Remarkably, the ADMR in this configuration replicates the $\cos^2\theta$ behavior at 100 K (Fig. 4(e)) and follows an identical temperature evolution, stabilizing as a well-defined $\sin^2\theta$ symmetry at 35 K (Fig. 4(f)). The observed uniformity in both twofold symmetry and temperature evolution stands in sharp contrast to the divergent responses expected for 1D systems, thereby unveiling the 2D nature of the surface transport. Although the specific microscopic mechanism governing the $\sin^2\theta$ dependence at low temperatures requires further clarification, its symmetry matches the expectations for the $NiS_2(001)$ surface. Notably, despite the microscopic evidence of spatially confined 1D conducting channels,[35] our observations suggest a limited contribution from these local features to the macroscopic transport.

To further differentiate intrinsic 2D transport from a potential superposition of oriented 1D filaments, which could collectively mimic 2D symmetry in macroscopic measurements, chemical doping was employed to introduce controlled disorder. Specifically, introduced impurities introduce atomic-scale impurities that act as random scattering centers, disrupting the periodic lattice potential. The theoretical basis for this approach lies in the scaling theory of localization, where the suppression of charge diffusion by disorder is fundamentally dependent on the dimensionality of the system.[52,53] In 1D systems, the metallic state is fundamentally unstable, where even slight perturbations can trigger strong Anderson localization or other phase transitions that quench metallic conduction.[54,55] Thus, if 1D channels governed the surface transport in NiS_2, slight doping could lead to a precipitous collapse of this transport behavior. Conversely, 2D systems could exhibit resilience when considering interactions

such as electron–electron coupling and thus manifest a gradual evolution of conductance under increasing disorder, which is exemplified in the 2D surface states of disordered Bi_2Se_3 films.[56,57] Consequently, the persistence of SC characteristics in NiS_2 under chemical doping provides a criterion to distinguish its dimensionality.

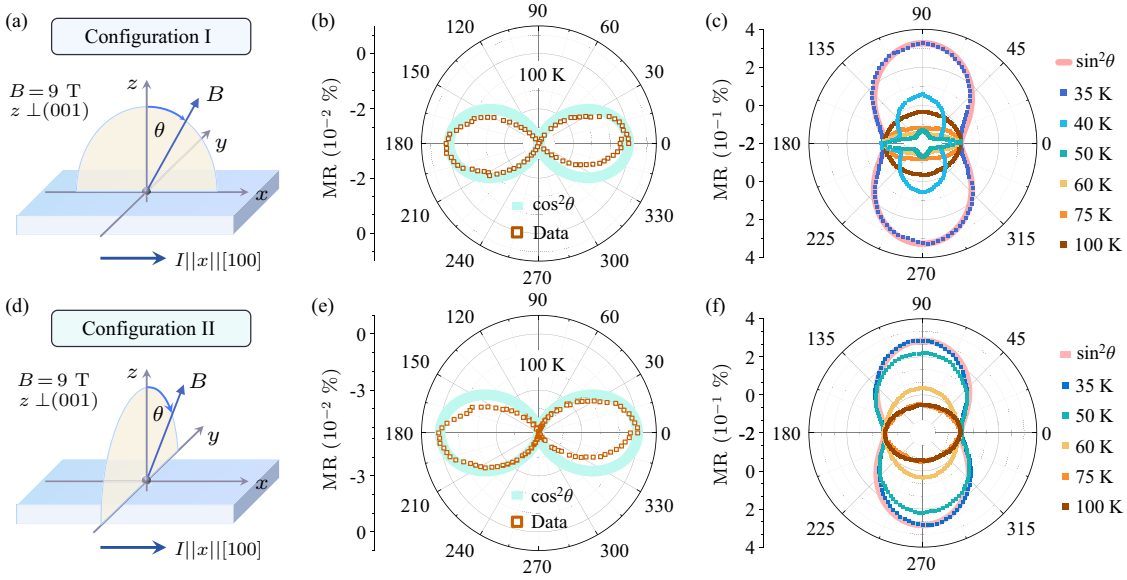


Fig. 4. Angle-dependent magnetoresistance with twofold symmetry in NiS_2. (a), (d) Schematic of measurement configurations, with B rotated in the xz-plane (configuration I) and yz-plane (configuration II), respectively. Current I is applied along the [100] direction (x-axis). (b), (c) ADMR polar plots for configuration I. (e), (f) Corresponding ADMR plots for configuration II. In both configurations, ADMR exhibits a pronounced twofold symmetry: it follows a $\cos^2\theta$ dependence at 100 K and evolves to a $\sin^2\theta$ dependence at 35 K. The identical symmetry and similar temperature evolution of ADMR across rotation planes indicate an in-plane isotropic response, consistent with the behavior of a 2D conducting system. The T-range from 100 K to 35 K falls in the plateau regime, and lower temperatures enable purer and stronger surface transport signals.

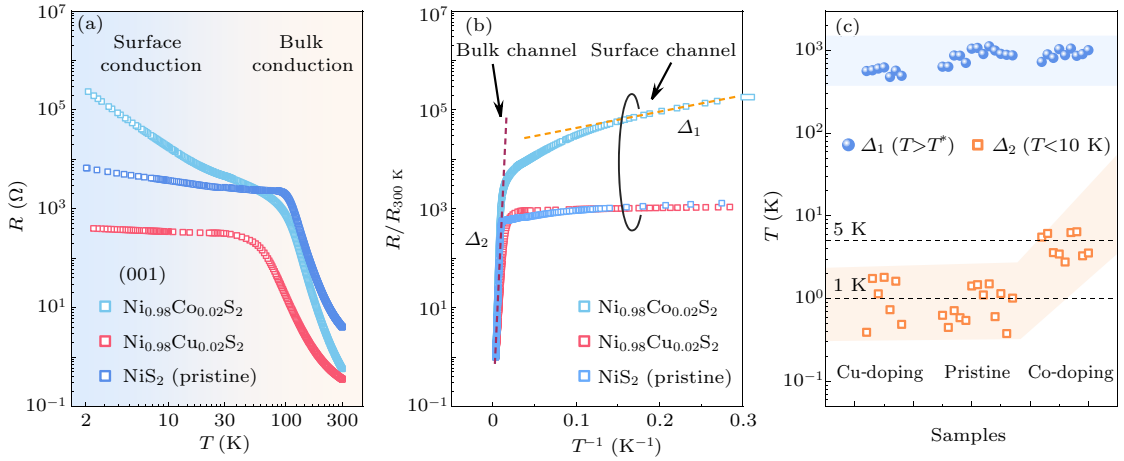


Fig. 5. Persistence of the surface conduction against chemical doping in NiS_2. (a) $R(T)$ profiles of pristine NiS_2 (S01 in Fig. 1) and Cu/Co-doped NiS_2 ($\sim 0.6\%$), showing the persistence of R-plateau at low temperatures. (b) Arrhenius plots of normalized R, $R/R_{300\ \mathrm{K}}$, from the data in (a). Linear fitting in high-temperature ($T > 200$ K) and low-temperature ($T < 10$ K) regimes yields excitation energies Δ_1 (bulk channel) and Δ_2 (surface channel), respectively. (c) Summary of Δ_1 and Δ_2 for a series of pristine and doped (~ 0.6 %) samples. The resilience of SC against doping-induced disorder contradicts the well-known fragility of 1D metallic systems, supporting 2D nature of the surface transport.

The $R(T)$ measurements for all samples were performed on mechanically as-cleaved (001) surfaces (Fig. 5(a)). For the $Ni_{0.98}Cu_{0.02}S_2$ crystal, the R-plateau remains evident and exhibits a saturation towards 0 K, indicating that the SC is preserved. Similarly, in $Ni_{0.98}Co_{0.02}S_2$, the plateau feature still persists although R increases by approximately two orders of magnitude from 100 K to 2 K. The corresponding Arrhenius plots clearly resolve the existence of a low-temperature surface contribution (Fig. 5(b)). Based on Arrhenius law, we extracted two activation energies: Δ_1 for bulk and an effective Δ_2 for the surface channel, with the latter signifying the continued dominance of SC at low temperatures. The evolution of these energies reflects the doping-induced shift in intrinsic properties instead of extrinsic surface artifacts (Table S1, supplementary information). Figure 5(c) summarizes the activation energies, Δ_1 and Δ_2, across a series of NiS_2 samples with controlled doping levels. The stability of Δ_1 confirms that the bulk insulating gap remains robust against slight substitution (atomic ratio $\sim 0.6\%$). More importantly, Δ_2 consistently falls within the thermal energy scale (< 10 K), underscoring

the persistence of the low-temperature transport channel and pointing toward its intrinsic 2D nature. Crucially, such results do not imply absolute stability, as increasing substitution levels inevitably escalate the degree of disorder within the system. At a higher Co-doping level ($Ni_{0.94}Co_{0.06}S_2$, see Fig. S3 in supplementary information), the intensified disorder eventually overwhelms the surface conduction, leading to a complete quenching of the plateau-like feature.

Collectively, these findings point toward a microscopic, intrinsic 2D conduction mechanism that fundamentally governs the low-temperature transport in NiS_2. To elucidate the microscopic origin of this 2D behavior, it is instructive to move beyond the 1D edge state scenario. Indeed, the spectroscopic evidence identifies point-like discrete conductive sites apart from 1D-like channels.[35] These point-like conductive spots likely combine to form a 2D conductive network, providing a basis for macroscopic signatures like the resistivity plateau and 2D-VRH conduction. In this picture, the network's connectivity ensures long-range transport, while the non-periodic spatial arrangement of these conductive sites provides conditions for VRH conduction.

In summary, our study points to a microscopic 2D characteristic for the surface conduction of NiS_2, thereby clarifying its intrinsic dimensionality uncertainty. This scenario is based on several transport signatures: the crossover from bulk thermally activated conduction to a 2D Mott-type VRH mechanism exhibiting a $T^{1/3}$ dependence; the in-plane conducting isotropy consistent with the identical twofold ADMR symmetries across orthogonal rotation planes; and the persistence of the surface conduction in the case of slight doping-induced disorder ($\sim 0.6\%$). This work deepens the understanding of surface transport in the Mott insulator NiS_2, which is essential for exploring emergent phenomena in Mott systems.

Acknowledgements

Project supported by the National Key Research and Development Program of China (Grant No. 2022YFA1403400), the National Natural Science Foundation of China (Grant Nos. 12595332 and 11974394), the Synergetic Extreme Condition User Facility (SECUF), and the Scientific Instrument Developing Project of CAS (Grant No. ZDKYYQ20210003).

References

[1] Van der Heide H, Hermel R, Vanbruggen C F and Haas C 1980 *J. Solid State Chem.* **33** 17
[2] Jobic S, Brec R and Rouxel J 1992 *J. Alloys Compd.* **178** 253
[3] Podberezskaya N V, Magarill S A, Pervukhina N V and Borisov S V 2001 *J. Struct. Chem.* **42** 654
[4] Gao M R, Zheng Y R, Jiang J and Yu S H 2017 *Acc. Chem. Res.* **50** 2194
[5] Robredo I, Schröter N B M, Reyes-Serrato A, Bergara A, de Juan F, Schoop L M and Vergniory M G 2022 *J. Phys. D: Appl. Phys.* **55** 304004
[6] Schröter N B M, Robredo I, Klemenz S, Kirby R J, Krieger J A, Pei D, Yu T, Stolz S, Kim T K, Dudin P, Manna K, Felser C, Parkin S S P, Vergniory M G, de Juan F and Strocov V N 2020 *Sci. Adv.* **6** eabd5000
[7] Zhang S, Wang Y, Zeng Q, Shen J, Zheng X, Yang J, Wang Z, Xi C, Wang B, Zhou M, Huang R, Wei H, Yao Y, Wang S, Parkin S S P, Felser C, Liu E and Shen B 2022 *Proc. Natl. Acad. Sci. USA* **119** e2208505119
[8] Zhang R, He Y, Chen K, Yang S, Sen S and Coey J M D 2023 *Proc. Natl. Acad. Sci.* **120** e2302466120
[9] Bither T A, Prewitt C T, Gillson J L, Bierstedt P E, Flippen R B and Young H S 1966 *Solid State Commun.* **4** 533
[10] Shi L, Liu Z, Li J, Zhang X, Wang N, Cui Q, Chen K, Liu Q, Yang P, Sun J, Wang B, Uwatoko Y, Sui Y, Yang H X and Cheng J 2022 *Phys. Rev. Mater.* **6** 014802
[11] Matsuura A Y, Shen Z X, Dessau D S, Park H, Thio T and Bennett J W 1996 *Phys. Rev. B* **53** R7584
[12] Imada M, Fujimori A and Tokura Y 1998 *Rev. Mod. Phys.* **70** 1039
[13] Reiss P, Friedemann S and Grosche F M 2022 *Phys. Rev. B* **106** 205131
[14] Day-Roberts E, Fernandes R M and Birol T 2023 *Phys. Rev. B* **107** 085150
[15] Xu H C, Zhang Y, Xu M, Peng R, Shen X P, Strocov V N, Chen M, Xie B P and Feng D L 2014 *Phys. Rev. Lett.* **112** 087603
[16] Semeniuk K, Chang H, Baglo J, Friedemann S, Tozer S W, Coniglio W A, Gamża M B, Reiss P, Alireza P, Leermakers I, McCollam A, Grockowiak A D and Grosche F M 2023 *Proc. Natl. Acad. Sci. USA* **120** e2301456120
[17] Mamiya K, Fujimori A, Sekiyama A, Imada S, Mizokawa T, Sugano S, Masuda K, Takeda H and Ogawa S 1998 *Phys. Rev. B* **58** 9611
[18] Thio T, Bennett J W and Thurston T R 1995 *Phys. Rev. B* **52** 3555
[19] Yano S, Louca D, Yang J, Chatterjee U, Bugaris D E, Chung D Y and Peng L 2016 *Phys. Rev. B* **93** 024409
[20] Zhou Y Z, Han X, Luo J, Wu D T, Fang A F, Shen B, Feng B J, Shi Y G, Yang J and Zhou R 2025 *Chin. Phys. Lett.* **42** 037303
[21] Yao X, Honig J M, Hogan T, Kannewurf C and Spalek J 1996 *Phys. Rev. B* **54** 17469
[22] Matsuura M, Endoh Y, Hiraka H, Yamada K, Mishchenko A S, Nagaosa N and Solovyev I V 2003 *Phys. Rev. B* **68** 094409
[23] El-Khatib S, Voigt B, Moore W, Pelc D, Das B, Greven M and Leighton C 2021 *Phys. Rev. Mater.* **5** 115003
[24] Kautz R L, Dresselhaus M S, Adler D and Linz A 1972 *Phys. Rev. B* **6** 2078
[25] Thio T and Bennett J W 1994 *Phys. Rev. B* **50** 10574
[26] Sarma D D, Krishnakumar S R, Weschke E, Schussler-Langeheine C, Mazumdar C, Kilian L and Kaindl G 2003 *Phys. Rev. B* **67** 155112
[27] Rao K D M, Bhuvana T, Radha B, Kurra N, Vidhyadhiraja N S and Kulkarni G U 2011 *J. Phys. Chem. C* **115** 10462
[28] El-Khatib S, Mustafa F, Egilmez M, Das B, Tao Y, Maiti M, Lee Y and Leighton C 2023 *Phys. Rev. Mater.* **7** 104401
[29] Clark C and Friedemann S 2016 *J. Magn. Magn. Mater.* **400** 56
[30] Hameed S, Voigt B, Dewey J, Moore W, Pelc D, Das B, El-Khatib S, Garcia-Barriocanal J, Luo B, Seaton N, Yu G, Leighton C and Greven M 2022 *Phys. Rev. Mater.* **6** 064601
[31] Bradlyn B, Elcoro L, Cano J, Vergniory M G, Wang Z, Felser C, Aroyo M I and Bernevig B A 2017 *Nature* **547** 298
[32] Xu Y F, Elcoro L, Li G W, Song Z D, Regnault N, Yang Q, Sun Y, Parkin S S P, Felser C and Bernevig B A 2021 arXiv:2111.02433 [cond-mat.mtrl-sci]
[33] Xu Y F, Elcoro L, Song Z D, Vergniory M G, Felser C, Parkin S S P, Regnault N, Mañes J L and Bernevig B A 2024 *Phys. Rev. B* **109** 165139
[34] Gao J C, Qian Y T, Jia H X, Guo Z P, Fang Z, Liu M, Weng H M and Wang Z J 2022 *Sci. Bull.* **67** 598
[35] Yasui Y, Shi L F, Zhang X, Hou J, Xia W, Xu Z, Yang P, Wang A, Liu Z, Shen J, Zhang H, Dong X, Uwatoko Y, Sun J, Wang B, Guo Y and Cheng J 2024 *Phys. Rev. B* **110** 045139
[36] Higo T and Nakatsuji S 2015 *J. Phys. Soc. Jpn.* **84** 053702
[37] Kikuchi K 1979 *J. Phys. Soc. Jpn.* **47** 484
[38] Crivillero M V A, Ghorbani Zavareh M, Manna K, Felser C, Parkin S S P, de Juan F, Schoop L M and Vergniory M G 2021 *Phys. Rev. Research* **3** 023162
[39] Eo Y S, Sun K, Kurdak Ç, Kim D J and Fisk Z 2020 *Phys. Rev. B* **101** 155109
[40] Evers F and Mirlin A D 2008 *Rev. Mod. Phys.* **80** 1355
[41] Anderson P W 2010 50 *Years of Anderson Localization* (Singapore: World Scientific Publishing Co. Pte. Ltd.) pp. 7–25
[42] Mott N F 1968 *J. Non-Cryst. Solids* **1** 1

[43] Hill R M 1976 *Phys. Status Solidi A* **34** 601

[44] Jovanovic V P, Alireza P, Friedemann S, Grockowiak A D, Ishida S, Hosono H, Tozer S W and Lonzarich G G 2010 *Phys. Rev. B* **81** 134520

[45] Jiang W, Robertson J L, Angelini P, Thompson J R and Christen D K 1994 *Phys. Rev. B* **49** 690

[46] Shklovskii B I and Efros A L 1984 *Electronic Properties of Doped Semiconductors* (Berlin: Springer) pp. 202–227

[47] Zhang L J, King I, Nasyedkin K, Chen P, Skinner B, Lunt R R and Pollanen J 2021 *ACS Appl. Electron. Mater.* **3** 2948

[48] Zhang S N, Wu Q S, Liu Y and Yazyev O V 2019 *Phys. Rev. B* **99** 035142

[49] Wang J L, Zhang S, Gao J C, Shen J, Wang Z, Liu E, Felser C, Shen B and Sun J 2019 *npj Quantum Mater.* **4** 1

[50] Fu B B, Yi C J, Zhang T T, Caputo M, Ma J Z, Gao X, Lv B Q, Kong L Y, Huang Y B, Richard P, Shi M, Strocov V N, Fang C, Weng H M, Shi Y G, Qian T and Ding H 2019 *Sci. Adv.* **5** eaau6459

[51] Chen F, Shang C, Jin Z, Zhao D, Wu Y P, Xiang Z J, Xia Z C, Wang A F, Luo X G, Wu T and Chen X H 2015 *Phys. Rev. B* **91** 205133

[52] Lee P A and Ramakrishnan T V 1985 *Rev. Mod. Phys.* **57** 287

[53] Abrahams E, Anderson P W, Licciardello D C and Ramakrishnan T V 1979 *Phys. Rev. Lett.* **42** 673

[54] Thouless D J 1977 *Phys. Rev. Lett.* **39** 1167

[55] Giamarchi T 2003 *Quantum Physics in One Dimension* (Oxford: Oxford University Press) pp. 270–302

[56] Spivak B, Oreto P and Kivelson S A 2010 *Rev. Mod. Phys.* **82** 1743

[57] Liao J, Ou Y, Feng X, Yang S, Lin C, Yang W, Wu K, He K, Ma X and Xue Q K 2015 *Phys. Rev. Lett.* **114** 216601